Nuclear Instruments and Methods in Physics Research B 119 (1996) 533–542

ELSEVIER

NIM B
Beam Interactions with Materials & Atoms

Comparison of TOF-ERDA and nuclear resonance reaction techniques for range profile measurements of keV energy implants

J. Jokinen *, J. Keinonen, P. Tikkanen, A. Kuronen, T. Ahlgren, K. Nordlund

Accelerator Laboratory, University of Helsinki, P.O. Box 43, FIN-00014 Helsinki, Finland

Received 17 May 1996; revised form received 26 July 1996

Abstract

A comparative study on the range measurements of keV energy implants by the Time-of-Flight Elastic Recoil Detection Analysis (TOF-ERDA) and conventionally used nuclear resonance reaction methods has been performed for 20–100 keV $^{15}N^{+}$ ions implanted into crystalline silicon. Range profiles of ^{15}N atoms were chosen because they can be measured accurately using a very strong and narrow resonance at $E_p = 429.6$ keV in the reaction $^{15}N(p,\alpha\gamma)^{12}C$ which provides a challenging test for other methods. The measured range profiles were simulated by molecular dynamics calculations where the interatomic N–Si pair potential is deduced from first principles calculations. The electronic stopping power for 20–100 keV nitrogen ions in silicon is deduced from the comparison of the measured and simulated range profiles. The results are discussed in the framework of the applicability of the TOF-ERDA technique for keV energy ion range measurements.

1. Introduction

Elastic Recoil Detection Analysis [1] (ERDA) [1,2] is a method by which the observation of recoiled target atoms yields the most direct information about target composition. In conventional ERDA measurements, recoiling atoms of different elements are separated with stopping foils. The foils cause, however, energy straggling and are not very easy to use when several elements need to be separated. Therefore, many different types of ERDA set-ups have been constructed [3–10]. One of the most promising techniques is Time-of-Flight ERDA (TOF-ERDA) [9–14] where, in addition to traditional energy measurement, time-of-flight over a known distance is measured for each atom. The mass of each detected atom can be calculated from the classical formula for kinetic energy. Furthermore, when the mass of a particle has been identified, the same equation with a tabulated accurate mass can be used to obtain the energy from the measured time-of-flight [15,16]. Accurate time calibration is more straighforward than energy calibration and using the time-of-flight signal instead of the signal from the energy detector can give a better energy resolution, especially for heavier particles. TOF-ERDA systems have been widely used mainly for analyzing thin films and layered structures.

In the Accelerator Laboratory we have systematically studied stopping power and employed range profiles of keV energy implants to deduce stopping power values at these energies [17–21]. In this work we present a TOF-ERDA measurement system and its application to depth profiling of ion-implanted concentration distributions. Range profiles of implanted ^{15}N in crystalline silicon (c-Si) were measured with the TOF-ERDA spectrometer and results are compared with those obtained with the 429 keV resonance in the reaction $^{15}N(p,\alpha\gamma)^{12}C$. This resonance reaction provides one of the best tools for the range measurements of keV energy light ions with the Nuclear Resonance Broadening (NRB) method [22]. The measured range profiles are compared with those obtained in Molecular Dynamics (MD) simulations [19]. From this comparison, the electronic stopping power of silicon for low energy nitrogen ions is deduced. In order to take into account the damage structure of implanted c-Si in the MD simulations, RBS channeling measurements were also performed.

2. Set up for TOF-ERDA measurements

2.1. Apparatus design

A schematic diagram of the TOF-ERDA measurement system constructed at the Accelerator Laboratory is shown

* Corresponding author. Fax: +358 9 191 40042; email: Janne.Jokinen@Helsinki.FI.

[1] Also known as Elastic Recoil Detection (ERD), Elastic Recoil Analysis (ERA), Forward Recoil Spectrometry (FRES) and Recoil Spectrometry (RS).

PII S0168-583X(96)00469-7

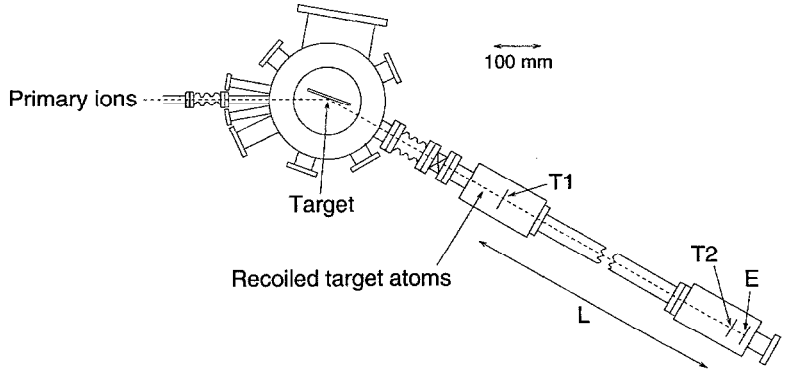

Fig. 1. Schematic diagram of the experimental configuration of TOF-ERDA measurements. Timing detectors T1 and T2 are used for measuring the time-of-flight over the flight path L. The energy detector is denoted by E.

in Fig. 1. A high-energy heavy ion beam from the 5 MV tandem accelerator EGP-10-II of the laboratory is directed to a 20-position target holder in the target chamber. The pressure in the chamber is kept lower than 1 μPa. The angle between the sample surface and the incident beam can be chosen freely. In standard measurements it has been 70°, measured from the normal of the sample surface. The angle between the direction of the ion beam and the direction where recoil atoms are detected can be selected in steps of 10° between 20° and 70°. In standard measurements it has been 40°. Measurements can also be done at backscattering angles.

The TOF-ERDA spectrometer system for recoiled particles consists of two timing detectors and an energy detector. The distance between the time detectors can be altered by changing the vacuum tube between them. The current timed flight length is 684 mm. An energy detector is located after the time detectors, in this study at a distance of 1243 mm from the target. The solid angle for the particle detection is 0.19 msr with the flight length and collimators used.

The design of both timing detectors follows that of Busch et al. [23]. Their structure can be seen in Fig. 2. Each timing detector consists of a thin carbon foil (currently 4.3 $\mu g/cm^2$ in the first and 22.8 $\mu g/cm^2$ in the second detector [24]) that emits secondary electrons when a recoil penetrates through it. Electric fields created by potential differences between the foil and grids accelerate and guide the electrons to a microchannel plate (MCP) [25]. The total transmission of the grids for the whole detector system is 72.3%. Secondary electrons from the foils are multiplied by two MCPs in series and subsequently collected by a metal anode. Voltages to foils, grids and MCPs are supplied by a 6.2 kV power source via a 31 MΩ resistor chain that is partially in vacuum. The MCPs are biased with a potential difference of 900 V and are

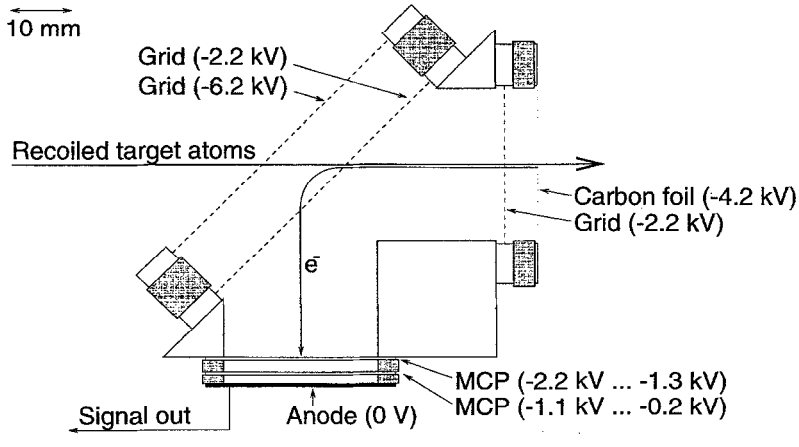

Fig. 2. Schematic diagram and principle of operation of a timing detector in the TOF-ERDA measurement system. Shaded components are of insulating teflon, supporting structure of aluminium and stainless steel.

separated from each other and from the anode by a small distance and a voltage of 200 V. The total-energy detector is an ion-implanted silicon detector from the EG&G Ortec Ultra series. This detector has an active area of 300 mm^2 and a depletion depth of 300 μm.

The timing and pulse-shaping electronics consist primarily of conventional NIM modules. The negative anode signals from the timing detectors are transformed to logical pulses in two constant fraction discriminator (CFD) units. Amplification of the anode signals is not necessary. The output signal from the CFD of the first timing detector is delayed in a coaxial cable and stops the conversion cycle of a time-to-amplitude converter (TAC). The output signal from the CFD of the second timing detector is used as a start pulse. This reversed start-stop order is used to minimize the dead-time of the TAC caused by a larger solid angle and therefore a higher count rate of the first timing detector. By choosing the length of the delay cable and the TAC time scale, a suitable time region can be obtained. Currently, flight times up to 210 ns are recorded. The signal from the energy detector is preamplified and amplified conventionally. The time and energy pulse-height signals are converted to digital form in two analog-to-digital converters (ADC) with a resolution of 4096×4096 channels and recorded with a Canberra MPA/PC multiparameter system. The coincidence between timing and energy signals is detected in the multiparameter system. In our standard analysis the MPA/PC system is used in a mode where time-of-flight and energy signals are regarded to be coincident if they arrive within 350 ns at the input.

2.2. Calibration and characteristics

For characterization of the TOF-ERDA system, several calibration spectra were measured. Beams of 4–15 MeV ^{1}H, ^{7}Li, ^{11}B, ^{12}C, ^{14}N, ^{15}N, ^{16}O, ^{19}F, ^{27}Al, ^{28}Si, ^{35}Cl, ^{63}Cu, and ^{69}Ga ions from the 5 MV tandem accelerator EGP-10-II of the laboratory were scattered from a thick tantalum target. The scattered ions were measured in a special mode where each detection of a particle, either in the time-of-flight or energy detector, was recorded in addition to the coincident events. The detection efficiency of the energy detector was assumed to be 100% for each element, and the relative efficiency of the whole spectrometer system was calculated as the ratio of (1) the number of coincidence events and (2) the number of particles detected by the energy detector. Measured average detection efficiency as a function of atomic number is shown in Fig. 3. For hydrogen detection, the efficiency is only a few percent, and was observed to be energy-dependent. The efficiency increases with increasing mass and depends only weakly on energy for heavier elements. At the energies relevant to the TOF-ERDA analysis, the detection efficiency can be assumed to be constant, and all elements heavier than hydrogen can be analyzed with a reasonable efficiency.

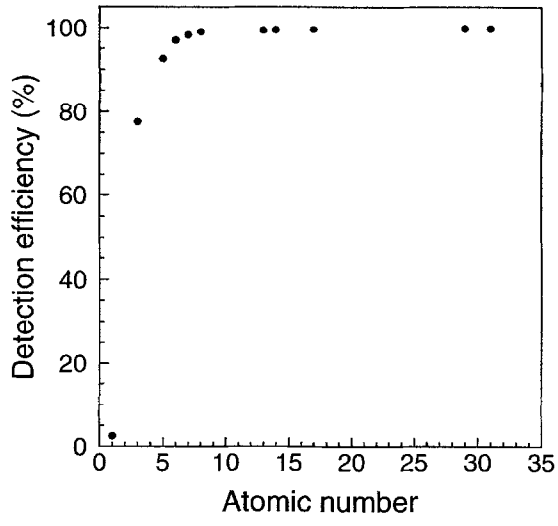

Fig. 3. Detection efficiency of the time-of-flight detector telescope in the current set-up as a function of atomic number. The efficiency is given relative to the efficiency of the energy detector.

In the time calibration the edge of each energy-TOF coincident spectrum corresponding to the shortest time-of-flight (signals from the sample surface) was used. Spectra were projected on the time axis and the slowing down in the first carbon foil was taken into account in the calibration. The time calibration curve did not depend on the particle mass or energy. A closely similar analysis for energy signals showed that the energy calibration curve was a somewhat nonlinear function of both the energy and mass of an atom. Therefore, the multivariate method of El Bouanani et al. [26] was used for energy calibration.

The time resolution of the TOF-ERDA system was determined by the use of the 5.4565 and 5.49921 MeV α-particles (28% and 72% relative intensities, respectively) emitted by a thin ^{238}Pu source [27]. The calculated time-of-flight difference of the α peaks is 164 ps for the geometry used. The peaks were not separated in the time-of-flight spectrum, and only one Gaussian line shape could be fitted to the composite peak in the spectrum. The time resolution for α particles is therefore better than 300 ps obtained at full width at half maximum (FWHM) of the peak, but worse than 164 ps. It is worth noting that for heavier particles the secondary electron yield from the carbon foils is higher, resulting in larger-amplitude timing signals, which would improve the time resolution for them, and compensate for the worsening of the resolution caused by the larger energy straggling in the first foil. The energy resolution of the semiconductor detector is 18 keV (FWHM) for α particles and becomes quickly poorer with heavier particles. The time resolution, however, is not particle-dependent to the same extent.

Mass and depth resolutions of TOF-ERDA systems have been studied in the literature for spectrometers closely

similar to that used in this work [11,14,16,26,28–31]. We analyzed mass and depth resolutions of our spectrometer for ^{16}O at the surface of pure quartz (SiO_2). Because the procedure requires similar kind of analysis methods as used in quantitative analysis of actual samples, the results are given in Section 4.1.

3. Measurements of ^{15}N-ion-implanted silicon samples

3.1. Samples

Two sets of samples were prepared by implanting 20, 40, 60, 80, and 100 keV $^{15}N^+$ ions into pure (100) silicon crystals at the 100 kV isotope separator of the laboratory. In order to avoid channeling of the implanted ions the Si(100) samples were tilted 8° relative to the beam and the ⟨100⟩ direction. The implantation dose was 1×10^{16} ions/cm^2 for the first set of the samples and 1×10^{15} ions/cm^2 for the second set of the samples.

3.2. TOF-ERDA measurements

The primary beam used to recoil target atoms consisted of 37 MeV $^{197}Au^{7+}$ ions supplied by the 5 MV tandem accelerator EGP-10-II of the laboratory. The beam current was about 7 nA (electric). The beam spot on the target was 3×3 mm^2. Each sample with the ion-implantation dose of 1×10^{16} ions/cm^2 was measured for about half an hour to obtain a reasonable counting statistics, and each sample with the implantation dose of 1×10^{15} ions/cm^2 for about an hour. In addition to the actual samples, a sample of pure quartz (SiO_2) was measured to study mass and depth resolutions.

The beam of ^{197}Au ions instead of lighter ones, e.g. ^{35}Cl, was chosen for the TOF-ERDA measurements in order to improve the depth resolution in the surface layer of the sample. The fact behind this is the high stopping power of materials for Au atoms. The high atomic number of the Au atoms results also in a large scattering cross section. Furthermore, Au atoms scattered from target atoms lighter than 126 u do not enter directly the TOF-ERDA spectrometer in the geometry used. This reduces the spectrometer dead-time radically, and radiation damage of the energy detector is prevented. In the current study these facts were considered to be more important relative to the disadvantages of using heavy primaries (greater radiation damage in the sample material and lower energy of light recoils due to smaller kinematic factors [2], resulting in worse energy and mass resolutions [31]).

3.3. NRB measurements

The concentration profiles of ^{15}N atoms were measured by NRB using the narrow ($\Gamma \approx 124$ eV [32]) 429.6 keV resonance in the reaction $^{15}N(p,\alpha\gamma)^{12}C$. The proton beams of about 1 μA were supplied by the 2.5 MV Van de Graaff accelerator of the laboratory. The beam energy resolution was about 1.5 keV (FWHM), corresponding to a depth resolving power of about 24 nm at the sample surface. The γ radiation ($E_\gamma = 4.43$ MeV) was detected in a 12.7 cm (diameter) × 10.2 cm NaI(Tl) crystal located 2 cm from the target and at an angle of 0° relative to the proton beam direction. The detector was shielded against the background radiation by 5 cm of lead. The beam was focused to a spot of 3×3 mm^2. The silicon sample was tilted 7° relative to the proton beam to avoid channeling of the probing beam [33]. The charge deposited by the probing beam was 20–100 μC per each measured point. The corresponding measuring time was between 30 min and 2 h for the whole range profile.

3.4. RBS channeling measurements

The crystallinity of the implanted samples was studied in RBS channeling measurements. The channeling 1.5 MeV $^4He^+$ ions were supplied by the 2.5 MV Van de Graaff accelerator of the laboratory. The angular divergence of the incident beam was less than 0.02°. Backscattered particles were analyzed with a 50 mm^2 Si(Li) detector located at 170° with respect to the incident beam and at a distance of 65 mm from the target. The particle detector subtended a solid angle of 7.9 msr. The energy resolution of the detector was 17 keV (FWHM). The samples were mounted on a precision goniometer, and the beam was aligned with respect to the ⟨100⟩ axis to give minimum backscattering yield. The concentrations of the displaced atoms were obtained by comparing spectra taken with an implanted sample aligned so that the ⟨100⟩ axis was in the beam direction (aligned implanted spectrum) with the same sample rotated so that a maximum yield was obtained (random spectrum), and with an unimplanted sample oriented so that the ⟨100⟩ axis was in the beam direction (aligned virgin spectrum). The relative ion doses for different spectra were obtained with an accuracy of better than 2% by using a beam chopper with a separate pulse analysis system.

4. Results

4.1. TOF-ERDA measurements

The first part of the analysis of the TOF-ERDA data obtained from the $^{15}N^+$ implanted samples (1×10^{16} ions/cm^2) was done with the CERN software package PAW (Physics Analysis Workstation) [34]. PAW is an analyzing and presentation environment that can handle multi-dimensional list data either interactively or in batch mode. One of the measured energy-TOF spectra is shown in Fig. 4.

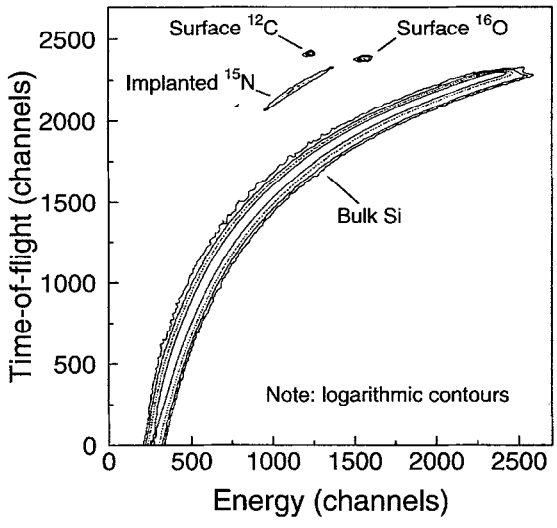

Fig. 4. Energy-TOF spectrum measured for the Si sample implanted with 1×10^{16} 60 keV ^{15}N ions/cm^2. Counts are shown with logarithmic contour curves. It should be noted that because the start-stop order is reversed in the time-of-flight measurement, the longest time is near the origin.

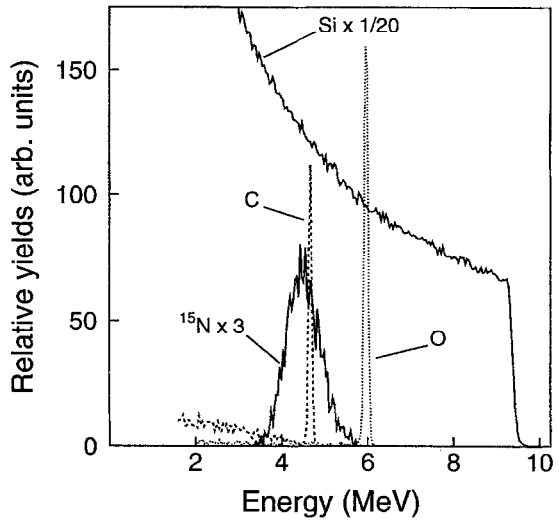

Fig. 6. Energy spectra for different elements calculated from the time-of-flight for the sample analyzed in Figs. 4 and 5. The resulting yields do not have the same physical meaning as in the raw data. The spectra are shown for the substrate material Si, contaminations of C and O, and for the implanted ^{15}N atoms.

By using linear time calibration and multivariate energy calibration [26], the mass of each detected particle was calculated using the nonrelativistic formula for the kinetic energy. The resulting three-parameter data was projected to TOF-mass spectra as illustrated in Fig. 5. From these spectra, detected ^{15}N, Si and C and O contaminants were easily separated by setting a window on the mass axis for each element. Because there were no overlap between different masses more precise methods [16,31] were not needed. Distributions of ^{15}N concentrations in the samples with the implantation dose of 1×10^{15} ions/cm^2 could not be deduced reliably because signals from bulk Si and O contaminations at the surface produced relatively high background in the N spectra and resulted in high statistical uncertainties of measured range profiles.

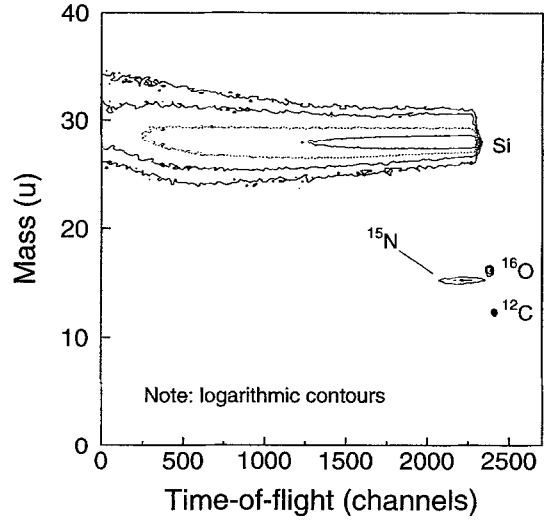

Fig. 5. TOF-mass spectrum calculated from the energy-TOF spectrum shown in Fig. 4. Counts are shown with logarithmic contour curves.

Data for each element were projected to time-of-flight spectra. Time information was used for further analysis because the depth resolution obtained from the time-of-flight measurements was better than the one from the energy measurements. The time spectra for each element were mapped to non-equidistant energy spectra by calculating the energy of each time channel using the tabulated atomic mass [15] and multiplying the yield in each channel with the Jacobian of the time-to-energy transformation [35]. The non-equidistant energy spectra were then mapped to equidistant energy spectra illustrated in Fig. 6. These energy spectra were used in calculating the concentration profiles as a function of depth.

In the analysis of the energy spectra, a computer program of the TOF-ERDA group at Tokyo Institute of Technology [36,37] was used to obtain the concentration distributions of the ^{15}N implants. The program was modified to use TRIM-95 stopping power [38] or an experimental stopping power instead of the original ZBL stopping power [39]. Even though at the projectile energies used (E_{lab} = 0.19 A MeV) screening effects cause deviation of the elastic scattering cross-section from the Rutherford cross-section they were neglected in the analysis. The screening was estimated to yield only a very small correc-

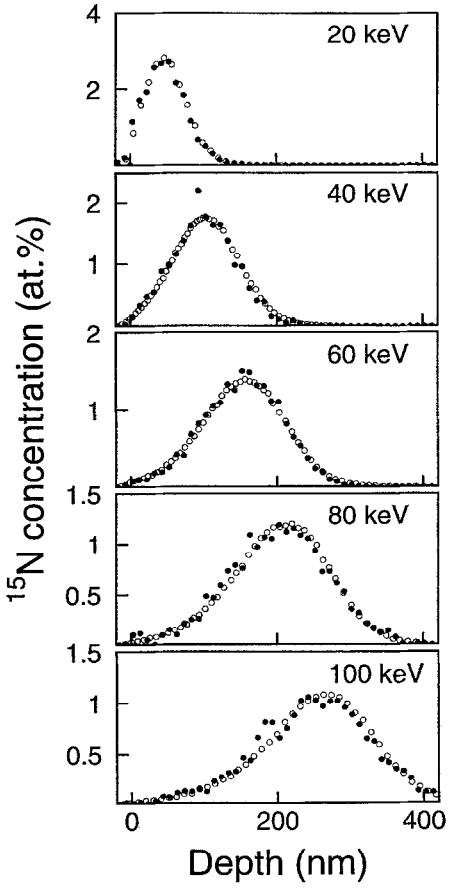

Fig. 7. Measured concentration profiles of ion-implanted ^{15}N as a function of depth for the samples with implantation dose of 1×10^{16} ions/cm^2. Implantation energy is given in each subfigure. TOF-ERDA profiles are shown with closed circles. NRB profiles are shown with open circles. The number of nitrogen atoms is normalized to 1×10^{16} atoms/cm^2 for all distributions.

tion factor, which can be considered constant (within statistical and other uncertainties) for the elements analyzed in the current study [40]. The main source of systematic errors in the analysis of TOF-ERDA data is the uncertainty of stopping power values used. In converting energy spectra into depth profiles, accurate stopping power values of Si for both the Au beam and the recoiling nitrogen atoms are needed in MeV energy region. The latter one has been determined experimentally [41]. Stopping power values for Au ions in the energy region used in the measurements are not known experimentally and the TRIM-95 values were used in the analysis. As illustrated in Fig. 7, the measured range profiles are observed to be in a good agreement with those obtained in the NRB measurements (see Section 4.2). Because the analyzed samples with the ion-implantation dose of 1×10^{16} ions/cm^2 were amorphous (see Section 4.3) the possible channeling effects of the Au beam or recoils were not expected to influence the results.

For characterization of the TOF-ERDA spectrometer, the mass resolution for ^{16}O was deduced. Oxygen was chosen because it is easy to measure with a SiO_2 calibration sample and its mass is similar to that of the mass of ^{15}N. The measured SiO_2 spectrum was transformed to a TOF-mass spectrum. A near-surface time-of-flight slice of oxygen counts was projected onto the mass axis and a Gaussian line shape was fitted to the mass spectrum. This resulted in a mass resolution of 0.4 u (FWHM). With increasing depth and mass the resolution becomes worse. The SiO_2 spectrum was converted to depth profiles with the method described above. By fitting a convolution of a step function with a Gaussian to the oxygen concentration profile, the depth resolution of 12 nm (FWHM of the Gaussian) at the sample surface was obtained.

4.2. NRB measurements

The concentrations of the ^{15}N atoms were obtained by comparison of γ-ray yields with those measured with a TiN standard. In the calculation of the depth scale, experimental electronic stopping power values of silicon for protons [42,43] were used. Results from measurements of ^{15}N range profiles are shown in Fig. 7 and 8. The measurements with the 1×10^{15} N/cm^2 and 1×10^{16} N/cm^2 samples showed only minor differences between these two sets of data as demonstrated in Fig. 8.

4.3. RBS channeling measurements

In order to study the damage in the nitrogen implanted c-Si samples, the concentrations of the Si atoms displaced from the lattice sites were obtained by comparing the spectra from the aligned virgin and random silicon sample with the spectra from the aligned implanted samples [44]. The depth scale was established by using the program Gisa3 [45]. It was observed that the samples with the ion-implantation dose of 1×10^{16} ions/cm^2 were completely amorphous. In the samples with ion-implantation dose of 1×10^{15} ions/cm^2, maximum concentrations of displaced atoms were observed to be about 20 at.%.

5. MD simulations

The measured range profiles shown in Figs. 7 and 8 were simulated using the molecular dynamics (MD) method and a simulation code developed in our laboratory [19]. The interatomic potential employed in the MD simulations was obtained by calculating the total energy of the N–Si dimer using density-functional theory (DFT) at the local-density approximation (LDA) level [46] using the DMol program package [47,48]. To obtain the interatomic force function, the total energy and its derivative were calculated

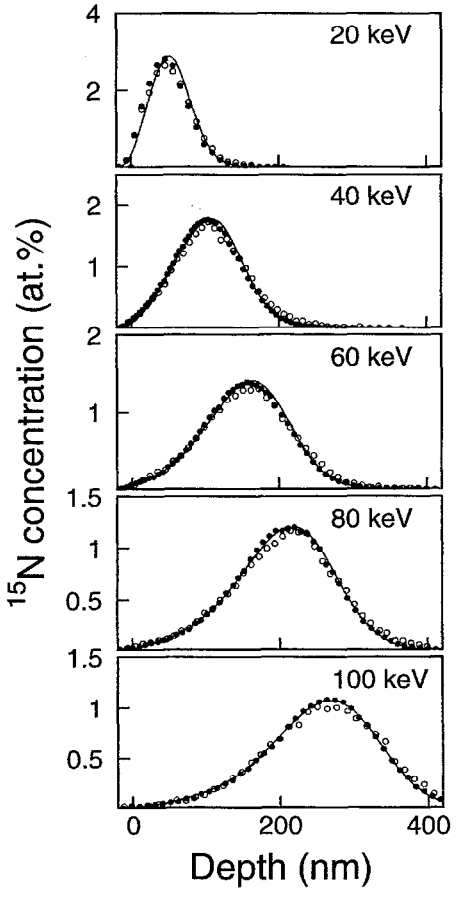

Fig. 8. Results from the NRB measurements. Implantation energy is given in each subfigure. Measured range profiles for the samples with the ion-implantation dose of 1×10^{16} ions/cm^2 are shown with closed circles, and for samples with the ion-implantation dose of 1×10^{15} ions/cm^2 with open circles. Simulated profiles for amorphous silicon are shown with solid lines. Simulated range profiles have been obtained with corrected stopping powers of Si for low-energy nitrogen ions and are convoluted with NRB depth resolution. The total number of implanted atoms is scaled to 1×10^{16} atoms/cm^2 for each distribution.

as a function of the interatomic distance r at dense intervals. To check the reliability of the DMol results, the total energy of the dimer was also calculated for a few internuclear distances using a fully numerical Hartree–Fock–Slater (X_α) method [49,50].

Comparison of the DMol and the numerical Hartree–Fock–Slater results showed that using the standard set of orbitals in generating the DMol basis functions [51] produces an interatomic potential which is about 3–4% stronger than the Hartree–Fock–Slater result in the energy region 0.1–10 keV. By augmenting hydrogenic orbitals [51] to the standard DMol orbitals for Si, good agreement (difference less than 1%) with the Hartree–Fock–Slater results was obtained. In the MD simulations, the repulsive potential and force were calculated by using a spline interpolation of the potential energy and force points obtained in the DMol calculations.

The electronic stopping power of silicon for keV energy nitrogen atoms was first obtained from the TRIM-95 code [38]. Range profiles were calculated for both crystalline and amorphous silicon. The atomic coordinates for the latter were based on ab initio MD simulations [52–54].

Before comparing the calculated range distributions with experimental results, they were convoluted with the experimental depth resolution. In the case of TOF-ERDA, resolution effects of the time-of-flight measurements, detector solid angle, multiple scattering of the Au beam and recoiling N ions, and electronic straggling of the Au beam and recoiling N ions were included [30,37,55]. In NRB measurements the energy resolution of the incoming proton beam and the electronic straggling of the probing beam determine the depth resolution. In calculating the elec-

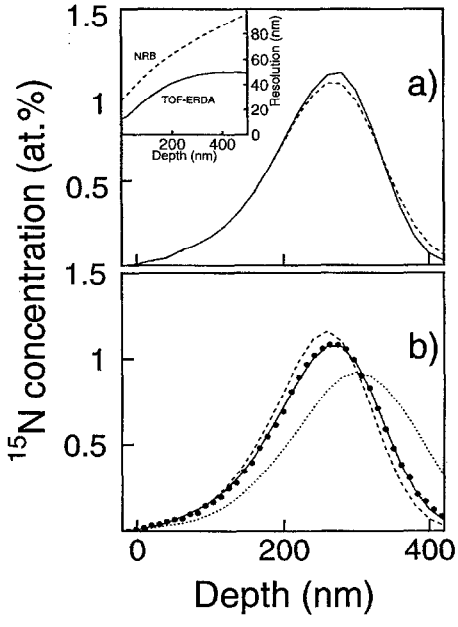

Fig. 9. Comparison of MD simulations with different parameters for a sample with 1×10^{16} 100 keV N^+ ions/cm^2. In (a) simulated profiles with corrected N stopping power for amorphous silicon are convoluted with depth resolutions of TOF-ERDA (solid line) and NRB (dashed line). The insert shows the calculated depth resolution of the methods as a function of depth. Resolution is defined as FWHM of a distribution obtained with the methods for an assumed delta-function concentration of ^{15}N. In (b) measured NRB profiles are shown with closed circles, distributions simulated for amorphous silicon with a dashed line (stopping power from TRIM-95) and for amorphous silicon with corrected N stopping power with a solid line. If the samples are assumed to have the structure of c-Si the range profile shown by the dotted line is obtained in the simulations using the corrected stopping power for low-energy N.

Table 1
Electronic stopping power for low-energy ^{15}N ions slowing down in Si as a function of ion velocity, as obtained from the current NRB range measurements (v_0 is Bohr velocity $= 2.188 \times 10^6$ m/s). Uncertainty of the stopping power is $\pm 4\%$. For comparison, the values given by the TRIM-95 program are listed

v/v_0	S_e (keV/nm)	
	current work	TRIM-95
0.22 [a]	0.148	0.158
0.24	0.158	0.169
0.26	0.167	0.179
0.28	0.177	0.189
0.30	0.186	0.199
0.32	0.196	0.209
0.34	0.205	0.219
0.36	0.214	0.229
0.38	0.223	0.238
0.40	0.231	0.247
0.42	0.240	0.257
0.44	0.248	0.266
0.46	0.257	0.275
0.48	0.265	0.284
0.50	0.274	0.293
0.52 [b]	0.282	0.301

[a] 18 keV ^{15}N atoms.
[b] 100 keV ^{15}N atoms.

tronic straggling the value given by the Bohr model [56] had to be multiplied by 0.8 to achieve a good agreement between measured and simulated range distributions. This is in a reasonable agreement with our previous result for 620 keV protons [18] and the theoretical estimations of Chu [57] and Yang et al. [58].

Depth resolutions of the NRB and TOF-ERDA techniques in the present measurements are compared in Fig. 9. In the case of TOF-ERDA measurements the effect of the finite solid angle of the spectrometer system and the time resolution of the TOF measurement are the main factors near the surface. Deeper in the sample the effect of multiple scattering of the beam and recoiling particles becomes dominant. For the NRB method, the beam energy resolution dominates near the surface but deeper in the sample the proton beam straggling quickly makes the depth resolution worse.

Good agreement between the NRB range distributions in targets with implantation dose of 1×10^{16} ions/cm^2 and simulated profiles at energies 40–100 keV was achieved when the TRIM-95 electronic stopping power was multiplied by 0.94. The corrected stopping power along with the TRIM-95 values is given in Table 1. In simulations the target was assumed to be amorphous. The discrepancy between the measured and simulated profiles at 20 keV energy cannot be explained by slowing-down conditions because the distributions are shifted with respect to each other. We interpret that the discrepancy is caused by surface erosion due to sputtering during the ^{15}N implantation. Since the implantations were carried out with equal doses, the largest erosion effect can be expected from the lowest energy implantations.

The electronic stopping power given by the TRIM-95 code has velocity dependence of the form $S_e \propto v^{0.75}$, where S_e is the stopping power and v the ion velocity. To our knowledge, the only experimental work published on electronic stopping power of silicon for nitrogen at the energy range of the present work is that of Grahmann and Kalbitzer [59]. They obtained a velocity proportional electronic stopping power ($S_e \propto v$). Simulations were also performed using this stopping power. The best fit was achieved by scaling the stopping power of Ref. [59] by 1.14. However, the agreement between the measured and simulated profiles was worse than in the case of TRIM-95 type stopping power.

It should be noted that in fitting the simulated profiles to NRB data both the correction factor of the electronic stopping power for N ions and the electronic straggling of the NRB proton beam can be determined because they affect the distributions in different ways. By scaling the stopping power essentially the depth scale of the profile is changed. The straggling only affects the width of the distribution. Consequently, the correction factor of the electronic stopping power giving the best fit between measured and simulated profiles was insensitive to the scaling factor of the proton beam straggling.

Simulated profiles for one of the implantation energies using both TRIM-95 and corrected ^{15}N stopping power values are shown with experimental results in Fig. 9. The differences between the calculated range profiles for amorphous and crystalline silicon are illustrated in Fig. 8. When the DMol repulsive potentials which had been calculated without addition of the hydrogenic orbitals (see above) were used in the analysis, the electronic stopping power obtained was roughly 6% smaller than the present results.

6. Discussion and conclusions

It was shown that the TOF-ERDA method can be used for range profile measurements of keV energy implants. The quality of the data obtained with the technique is comparable to the quality obtained for nitrogen with NRB in the reaction $^{15}N(p,\alpha\gamma)^{12}C$ at the 429 keV resonance which is one of the best resonances available. Reactions for other elements have either smaller cross sections or yield poorer depth resolution. In addition, TOF-ERDA measurements analyze several elements and isotopes simultaneously, and can replace NRB measurements in most cases. This is true especially when the reactions used in NRB have low cross sections or broad resonances, or do not have suitable resonances, as in the case of depth profiling of oxygen. However, it is difficult to obtain with

TOF-ERDA as good counting statistics as in NRB with the largest cross sections. Furthermore, one of the main difficulties with TOF-ERDA is that its accurate use requires knowledge of stopping powers of both the probing ions and the detected recoiled ions. On the other hand, if the concentration depth profile is known, TOF-ERDA measurements can be used in obtaining the stopping power values for either probing or recoiling ions.

In conclusion, it was demonstrated that range profiles of keV nitrogen atoms can be measured as reliably with TOF-ERDA as with NRB, when the implantation doses are of the order of 1×10^{16} ions/cm^2 or larger. The range profiles for implantation doses of the order of 1×10^{15} ions/cm^2 could be analyzed if long measurement times (several hours per sample) could be tolerated. By using Au atoms in the probing beams, the depth resolution of TOF-ERDA deep inside the sample is better than that of NRB in spite of the fact that the narrow 429 keV resonance of the reaction ^{15}N(p,$\alpha\gamma$)^{12}C is used in NRB. The accuracy of the NRB results depends on the stopping power of the probing protons, the accuracy of the TOF-ERDA results depends on the stopping power of both incoming Au and recoiling N atoms. Stopping powers of silicon known experimentally for protons and nitrogen atoms indicate that the stopping power for gold in the velocity region of $v/v_0 = 2.44$–2.75 ($E = 29$–37 MeV) is in agreement with the TRIM-95 values. Range profiles obtained with MD and DMol calculations for 20–100 keV N ions showed that the electronic stopping power values given by the TRIM-95 program for N are 6% too large.

Acknowledgements

This work was supported by the Academy of Finland and Finnish Technology Development Centre (TEKES). We want to thank Dr. Harry J. Whitlow for much advice and Prof. Eiichi Arai for supplying a copy of the analysis program.

References

[1] J. L'Ecuyer, C. Brassard, C. Cardinal, J. Chabbal, L. Deschênes, J. P. Labrie, B. Terreault, J. G. Martel and R. St.-Jacques, J. Appl. Phys. 47 (1976) 381.
[2] W. M. A. Bik and F. H. P. M. Habraken, Rep. Prog. Phys. 56 (1993) 859.
[3] M. Petrascu, I. Berceanu, I. Brancus, A. Buta, M. Duma, C. Grama, I. Lazar, I. Mihai, M. Petrovici, V. Simion, M. Mihaila and I. Ghita, Nucl. Instr. and Meth. B 4 (1984) 396.
[4] W. M. Arnold Bik, C. T. A. M. de Laat and F. H. P. M. Habraken, Nucl. Instr. and Meth. B 64 (1992) 832.
[5] B. L. Cohen, C. L. Fink and J. H. Degnan, J. Appl. Phys. 43 (1972) 19.
[6] S. S. Klein, Nucl. Instr. and Meth. B 15 (1986) 464.
[7] C. R. Gossett, Nucl. Instr. and Meth. B 15 (1986) 481.
[8] S. S. Klein and H. A. Rijken, Nucl. Instr. and Meth. B 66 (1992) 393.
[9] R. Groleau, S. C. Gujrathi and J. P. Martin, Nucl. Instr. and Meth. 218 (1983) 11.
[10] J. P. Thomas, M. Fallavier, D. Ramdane, N. Chevarier and A. Chevarier, Nucl. Instr. and Meth. 218 (1983) 125.
[11] H. J. Whitlow, G. Possnert and C. S. Petersson, Nucl. Instr. and Meth. B27 (1987) 448.
[12] E. Arai, H. Funaki, M. Katayama, Y. Oguri and K. Shimizu, Nucl. Instr. and Meth. B 64 (1992) 296.
[13] P. Goppelt, B. Gebauer, D. Fink, M. Wilpert, Th. Wilpert and W. Bohne, Nucl. Instr. and Meth. B 68 (1992) 235.
[14] J. W. Martin, D. D. Cohen, N. Dytlewski, D. B. Garton, H. J. Whitlow, and G. J. Russell, Nucl. Instr. and Meth. B 94 (1994) 277.
[15] G. Audi and A. H. Wapstra, Nucl. Phys. A 595 (1995) 409.
[16] M. Hult, H. J. Whitlow and M. Östling, Appl. Phys. Lett. 60 (1992) 219.
[17] P. Torri, J. Keinonen and K. Nordlund, Nucl. Instr. and Meth. B 84 (1994) 105.
[18] J. Keinonen, A. Kuronen, K. Nordlund, R. M. Nieminen and A. P. Seitsonen, Nucl. Instr. and Meth. B 88 (1994) 382.
[19] K. Nordlund, Comp. Mat. Sci. 3 (1995) 448.
[20] K. Nordlund, J. Keinonen, E. Rauhala and T. Ahlgren, Phys. Rev. B 52 (1995) 15170.
[21] P. Haussalo, K. Nordlund and J. Keinonen, Nucl. Instr. and Meth. B 111 (1996) 1.
[22] J.-P. Hirvonen, in: Handbook of Modern Ion Beam Materials Analysis, eds. J. R. Tesmer and M. Nastasi (Materials Research Society, Pittsburgh, 1995).
[23] F. Busch, W. Pfeffer, B. Kohlmeyer, D. Schüll and F. Pühlhoffer, Nucl. Instr. and Meth. 171 (1980) 71.
[24] Supplied by The Arizona Carbon Foil Co., Inc.
[25] Supplied by Galileo Electro-Optics Corporation.
[26] M. El Bouanani, M. Hult, L. Persson, E. Swietlicki, M. Andersson, M. Östling, N. Lundberg, C. Zaring, D. D. Cohen, N. Dytlewski, P. N. Johnston, S. R. Walker, I. F. Bubb and H. J. Whitlow, Nucl. Instr. and Meth. B 94 (1994) 530.
[27] C. M. Lederer and V. S. Shirley, eds., in: Table of Isotopes, 7th Ed. (Wiley, New York, 1978).
[28] J. P. Thomas, M. Fallavier and A. Ziani, Nucl. Instr. and Meth. B 15 (1986) 443.
[29] H. J. Whitlow, B. Jakobsson and Division L. Westerberg, Nucl. Instr. and Meth. A 310 (1991) 636.
[30] E. Arai, A. Zounek and N. Sekino and K. Saito, Nucl. Instr. and Meth. B 89 (1994) 149.
[31] M. Hult, M. El Bouanani, L. Persson, H. J. Whitlow, M. Andersson, C. Zaring, M. Östling, D. D. Cohen, N. Dytlewski, I. F. Bubb, P. N. Johnston and S. R. Walker, Nucl. Instr. and Meth. B 101 (1995) 263.
[32] T. Osipowics, K.P. Lieb and S. Brusserman, Nucl. Instr. and Meth. B 18 (1987) 232.
[33] J. D. Mader, R. W. Michelmann, F. Ditrói and K. Bethge, Nucl. Instr. and Meth. B 99 (1995) 440.
[34] Physics Analysis Workstation, Application Software Group, Computing and Networks Division, CERN (1995).
[35] M. H. Mendenhall and R. A. Weller, Nucl. Instr. and Meth. B 47 (1990) 193.
[36] E. Arai, H. Funaki, M. Katayama and K. Shimizu, Nucl. Instr. and Meth. B 68 (1992) 202.

[37] E. Arai, private communication.
[38] J. F. Ziegler and J. P. Biersack, TRIM-95 computercode, version 95.9.
[39] J. F. Ziegler, J. P. Biersack and U. Littmark, The Stopping and Range of Ions in Solids (Pergamon Press, New York, 1985).
[40] H. H. Andersen, F. Besenbacher, P. Loftager and W. Möller, Phys. Rev. A 21 (1980) 1891.
[41] U. Bussman, N. Hecking, K. F. Heidemann and E. Te Kaat, Nucl. Instr. and Meth. B 15 (1986) 105.
[42] P. Mertens and P. Bauer, Nucl. Instr. and Meth. B 33 (1988) 133.
[43] D. C. Santry and R. D. Werner, Nucl. Instr. and Meth. 188 (1981) 211.
[44] L. Feldman, J. Mayer and S. T. Picraux, Materials Analysis by Ion Channeling (Academic Press, New York, 1982) p. 118.
[45] J. Saarilahti and E. Rauhala, Nucl. Instr. and Meth. B 64 (1992) 734.
[46] R. O. Jones and O. Gunnarsson, Rev. Mod. Phys. 61 (1989) 689.
[47] J. Delley, J. Chem. Phys. 92 (1990) 508.
[48] DMol is a trademark of Bio Sym. Inc., San Diego, California, USA.
[49] L. Laaksonen, P. Pyykkö and D. Sundholm, Comp. Phys. Rep. 4 (1986) 313.
[50] K. Nordlund, D. Sundholm and N. Runeberg, to be published.
[51] DMol User Guide, V. 2.3.5, Biosym Technologies Inc., San Diego, California, 1993.
[52] D. A. Drabold, P. A. Fedders, O. F. Sankey and J. D. Dow, Phys. Rev. B 42 (1990) 5135.
[53] P. A. Fedders, D. A. Drabold and S. Klemm, Phys. Rev. B 45 (1992) 4048.
[54] D. A. Drabold, private communication.
[55] A. Turos and O. Meyer, Nucl. Instr. and Meth. B 4 (1984) 92.
[56] N. Bohr, Mat. Fys. Medd. Dan. Vid. Selsk. 18 (1948).
[57] W. K. Chu, Phys. Rev. A 13 (1976) 2057.
[58] Q. Yang, D. J. O'Connor and Z. Wang, Nucl. Instr. and Meth. B 61 (1991) 149.
[59] H. Grahmann and S. Kalbitzer, Nucl. Instr. and Meth. 132 (1976) 119.